Lab on a Chip

PAPER

View Article Online
View Journal | View Issue

Cite this: *Lab Chip*, 2019, **19**, 1296

An electric-field-dependent drop selector†

Jinlong Yang,[a] Dehui Wang,[a] Hailong Liu,[b] Linxian Li,[c] Longquan Chen,[d] Hong-Ren Jiang*[e] and Xu Deng*[a]

Received 24th December 2018,
Accepted 22nd February 2019

DOI: 10.1039/c8lc01403e

rsc.li/loc

Drop manipulation on hydrophobic surfaces is of importance in lab-on-a-chip applications. Recently, superhydrophobic surface-assisted lab-on-a-chips have attracted significant attention from researchers due to their advantages of contamination resistance and low adhesion between the drop and the surface during manipulation. However, control over both static and dynamic interactions between a drop and a superhydrophobic surface has been rarely achieved. In this study, we designed an electric-field-dependent liquid-dielectrophoresis force to manipulate a drop on a superhydrophobic surface. This type of control has been found to be fast in response, bio-friendly, convenient, repeatable, and energy efficient. Moreover, the adhesion force and rebounding for both the static and the dynamic interactions between the drop and the surface under an electric field have been explored. It was found that the adhesion force could be reversibly tuned three-fold without breaking the Cassie–Baxter state. Rebounding experiments showed a close to linear relation between energy dissipation and the applied voltage. This relation was used to tune the on-demand behaviors of a drop on a surface in a proof-of-concept experiment for drop sorting. This electric-field-dependent drop manipulation may have potential applications in digital microfluidics, microreactors and advanced lab-on-a-drop platforms.

1. Introduction

Control over the interactions of drops on surfaces is essential for not only the basic understanding of various processes, ranging from daily life to cooling and coating,[1–3] but also a variety of viable applications such as in digital microfluidics.[4–7] Recently, due to their excellent liquid-repellence, superhydrophobic surfaces have received significant attention as a promising substrate for controlling the behaviors of drops.[8–11] In recent years, the dynamic behaviour, including rebounding, jumping, self-cleaning, and cooling, and the interactions between the drop and the superhydrophobic surface have been extensively studied;[12–15] however, these surfaces have constant wetting properties over a certain period of time that restrict the real-time tunable wettability of these surfaces after fabrication. In practical applications, such as in digital microfluidics, active control of the wettability is more desirable. Although extensive studies have been reported on superhydrophobic surfaces with static wetting properties, dynamic and reversible control over the wettability of these surfaces have been less often studied.

To actively control the interactions between the drop and the surface, which are mainly determined by the wettability of the surface, the development of adaptive and intelligent superhydrophobic surfaces is desired. Extensive strategies, including regulations of chemical composition and structural roughness[16–19] and external stimulation to conquer the energy barrier,[20–24] have been reported to design and fabricate smart surfaces with adjustable wettability. Compared to the passive method of changing the surface properties, external stimulation is of significant value for actively controlling the drop behavior in the process. Heat,[24,25] light,[22,26] pH,[24] magnetic field,[23,27] and electric field[21,28–30] have been commonly used as external stimuli in the regulation of surface wettability. Among them, electrowetting, generated from an electric field, stands out due to its reliability, high efficiency, and fast response.[21,29–31] Through the movement of free charge, electrowetting modulates the contact angle and thus actuates the drop. The variation of the contact angle (φ) in response to the applied voltage (U) is generally described by the Young–Lippmann equation ($\cos\varphi = \cos\varphi_{eq} + CU^2/2\gamma$).[30] Herein, φ_{eq} is the equilibrium contact angle at zero voltage, C is the capacitance per unit area, and γ is the surface tension of the liquid. With good stability in the modulation of the

[a] *Institute of Fundamental and Frontier Sciences, University of Electronic Science and Technology of China, Chengdu, China. E-mail: dengxu@uestc.edu.cn*
[b] *School of Energy and Power Engineering, Jiangsu University, Zhenjiang, China*
[c] *Ming Wai Lau Centre for Reparative Medicine, Karolinska Institute, Hong Kong, China*
[d] *School of Physics, University of Electronic Science and Technology of China, Chengdu, China*
[e] *Institute of Applied Mechanics, National Taiwan University, Taipei, 106, Taiwan. E-mail: hrjiang@iam.ntu.edu.tw*

† Electronic supplementary information (ESI) available. See DOI: 10.1039/c8lc01403e

contact angle, electrowetting has been widely applied in applications such as in electronic displays, adaptive optical lenses, and microfluidics;[32–34] despite the merits of electrowetting, the requirement of conducting liquids and the direct contact between the liquid and electrodes may limit the applications of electrowetting, especially in the dynamic manipulation of liquid drops. Therefore, it is highly desirable to fabricate customized surfaces with the ability to statically and dynamically realize the on-demand behaviors of drops.

Recently, dielectrowetting has been proposed and demonstrated under different conditions mainly for contact angle actuation.[28,35–37] In the case of interdigitated finger electrodes underneath an insulating layer, dielectrowetting employs a non-uniform electric field, which penetrates the layer until the liquid drop, to generate a liquid-dielectrophoresis (L-DEP) force by the polarization of neutral matter.[35,36] Unlike electrowetting, dielectrowetting is independent of the liquid conductivity and thus can be used to control the contact angle of the drop in a number of applications in microfluidics.[28,36,38] However, compared to the extensive studies reported on contact angle manipulation on a smooth hydrophobic surface, few studies have been attempted to exploit dielectrowetting on a superhydrophobic surface.

In this study, we report an intelligent superhydrophobic surface with on-demand adjustable wettability controlled by dielectrowetting. An electric-field-dependent L-DEP force was harnessed to control the interaction between the drop and the superhydrophobic surfaces. Taking advantages of the superhydrophobic surface and dielectrowetting, we showed that both the adhesion force and the rebounding of the drop could be efficiently tuned on a superhydrophobic surface by the actuation voltage of 0–49 V. To demonstrate the possible applications of dielectrowetting on superhydrophobic surfaces, we have demonstrated a proof-of-concept experiment of drop sorting, which may have potential applications in digital microfluidics, micro-reactors and advanced lab-on-a-drop platforms.

2. Experimental

2.1. Design of the superhydrophobic interdigitated array (IDA) chips

The schematic of the experimental setup is shown in Fig. 1a. An IDA chip (MECART, China) was coated with a superhydrophobic coating, which was made by chemical vapor deposition of silica on candle soot followed by fluorination as previously reported.[8] Briefly, candle soot, consisting of carbon particles, was finely deposited on the chip by holding the substrate above the flame of a paraffin candle. The soot layer was then coated by a silica shell *via* chemical vapor deposition (CVD) using tetraethoxysilane (Sigma Aldrich, 98%) and an aqueous ammonia solution (TCI, 28%). After the silica shell was coated, the carbon core was removed by plasma. To reduce the surface energy, the surface was coated with trichloro(1*H*,1*H*,2*H*,2*H*-perfluorooctyl)silane (Sigma Aldrich, 97%) by CVD. The superhydrophobic surface featured the water apparent contact angle of 166° ± 1° and a roll-off angle less than 5°. The IDA chip was constructed by 25 sets of interdigitated gold finger electrodes with a thickness of 100 nm on the silicon substrate (6 × 4 mm). Both the width and spacing of the electrodes were 40 μm. Then, a superhydrophobic coating with a thickness of 10 μm was integrated on the chip (Fig. S1†). The morphology of the

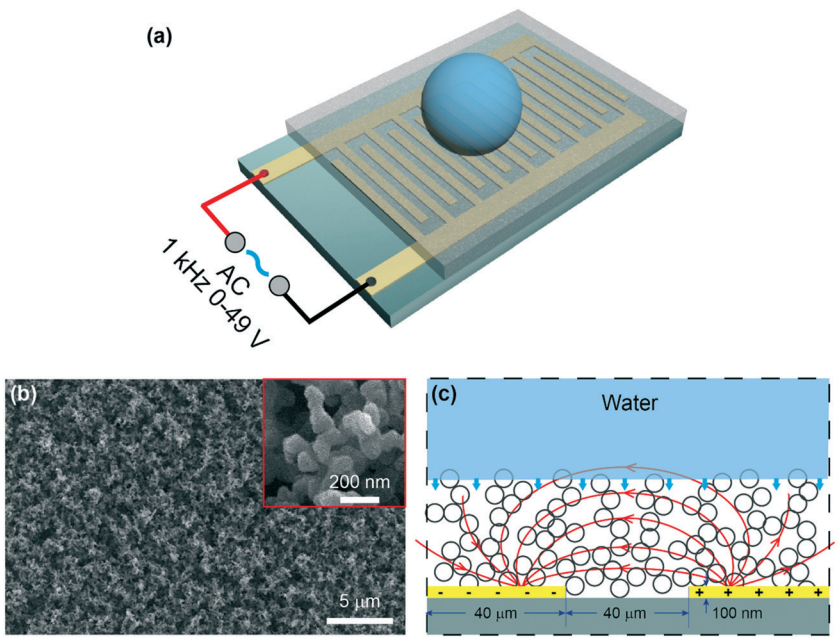

Fig. 1 Experimental setup. (a) Schematic of the IDA electrodes covered with the superhydrophobic coating. (b) Scanning electron microscopy (SEM) images of the superhydrophobic coating. (c) Side view of the IDA chip under an electric field.

superhydrophobic surface was characterized by a scanning electron microscope (FEI, Inspect F50, Japan). The coating featured nano-sized particles with an outer radius of ~60 nm and porosity with an average pore space of ~1 μm (Fig. 1b).

2.2. Generation of the electric field

To generate a non-uniform electric field between the finger electrodes, alternating current (AC) voltages were supplied to the circuit (Fig. 1a and c), allowing deeper penetration of the electric field into the liquid than the DC voltages.[28] A sinusoidal signal was generated at the frequency of 1 kHz by a function generator (Tektronix, AWG 520, USA) and amplified by an amplifier (NF corporation, HSA4011, Japan). Voltages (root-mean-square values) ranging from 0 to 49 V were used throughout the experiments. When a voltage was applied, a highly localized electric field (Fig. 1c) was generated above the electrodes.[36,39] Note that the dielectrowetting system is open circuit, and thus, the current is negligible; this makes the device energy efficient.

2.3. Adhesion force, apparent contact angle, and roll-off angle measurement

The adhesion force (F_a) was measured using a high-sensitivity microelectromechanical balance system (Data-Physics, K100C, Germany). A 3 μL deionized (DI) water drop was suspended on a needle (0.5 mm in outer diameter), which was connected to a force sensor. The superhydrophobic IDA chip was placed on a horizontal table underneath the drop. During the measurement of the adhesion force, the IDA chip was slowly moved upward such that it contacted the water drop and then moved down at the constant speed of 0.02 mm s^{-1}; during this process, the balancing force gradually increased to its maximum and then sharply reduced to zero. The maximum force before detachment was marked as the adhesion force. The apparent contact angle (φ_a) and roll-off angle (φ_r) were measured *via* the Data-Physics OCA 50 contact angle system using a 5 μL water drop. All the experiments were conducted at ambient temperature and repeated at least three times.

2.4. Drop rebounding experiments

The superhydrophobic IDA chip was positioned on a horizontal stage. A 3 μL water drop impacted the superhydrophobic surface, and the velocity (v) changed from 0.2 to 0.4 m s^{-1}; moreover, the corresponding Weber number ($We = \rho D v^2/\gamma$) changed from 1 to 4, where ρ, D and γ are the density, diameter and surface tension of the droplet, respectively. The impact process was investigated using a high-speed camera (Photron, Fastcam, Japan) at 5000 fps. The obtained videos were further processed using the custom-programmed MATLAB (Math_Works Inc., USA) algorithm.

2.5. Simulation of the electric field

Simulation of the electric field was conducted using the commercial software COMSOL Multiphysics (Version 5.3a). The dimensions used in the simulation were exactly the same as those used in the fabrication (Fig. 1c, Fig. S2†). A vertical plane at the center of the water drop was selected as the computational domain (please refer to Fig. S2† for details of the simulation). The physical properties of the materials used in the simulation are summarized in Table S1.†

3. Results and discussion

3.1. Manipulation of the static interaction between the drop and the surface under an electric field

To demonstrate the capacity of the device to control the adhesion force (F_a), we first measured F_a in response to a series of voltages. A schematic of the adhesion force measurement can be found in Fig. 2a and Video S1.† The adhesion force at zero voltage was around 7 μN, consistent with the small adhesion force on superhydrophobic surfaces reported in other studies.[8] The adhesion force monotonically increased when the voltage was elevated and reached almost three-fold at 49 V (Fig. 2b). The images in Fig. 2b show a comparison of the drop profiles upon detachment at the voltages of 0 V, 21 V, and 42 V. The force exerted on the droplet is reflected by the shape of the drop. Without voltage, the drop slightly deformed; this indicated a small hysteresis of the interaction between the drop and the surface. By increasing the applied voltage, the detaching force as well as the detaching distance increased; this was indicated by the deformation of the drop. Although there was a significant increase in the adhesion force, the apparent contact angle (φ_a) only slightly decreased from 166° at 0 V to 159° at 49 V (Fig. 2c). This monotonic increase in the adhesion force and slight decrease in the apparent contact angle suggested that the adhesion force could be modulated from 7 μN to 21 μN by a relatively low voltage, *i.e.*, 49 V. The roll-off angles in response to the voltage (Fig. 2c) followed the same trend of the adhesion force curve, reaching a maximum value close to 11° at the voltage of 49 V. This was not unexpected since the increasing L-DEP force derived from the electric field contributed to the growth of the roll-off angle, namely, the hysteresis of the contact angle. Notably, the manipulation of the adhesion force under the applied voltage was reversible (Fig. 2d); this enabled the device to repeatedly regulate the adhesion force in practical applications.

During the manipulation of the adhesion force, the electric field was mostly confined on the drop surface due to the exponential decay in the water phase.[36] We confirmed this by simulating the electric field with a drop sitting on a superhydrophobic surface (Fig. 2e). The electric field was highly confined inside the porous structure and hardly penetrated inside the drop; this was is in accordance with the findings reported in the literature.[36,40] Since the drop only touched the surface by a small area and the electric field only affected the air-liquid surface of the trapped liquid at the contact area, a negligible electric field penetrated the drop. This

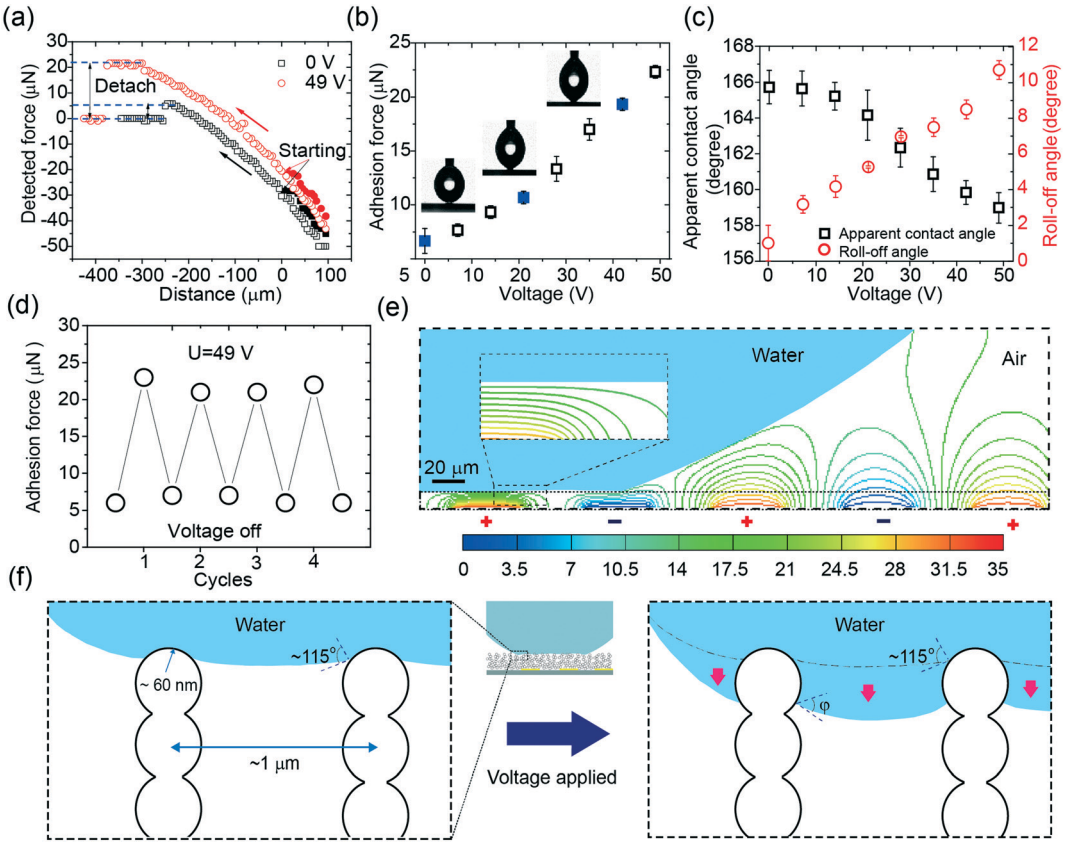

Fig. 2 Static interactions between a drop and surface under an electric field. (a) Adhesion force measurement. (b) Adhesion force of the drop on the superhydrophobic surface at different applied voltages. Insets show the images of the drops obtained upon detachment at the voltages of 0 V, 21 V, and 42 V. (c) Apparent contact angle and roll-off angle of the drop in response to the applied voltages. (d) Repeatability of the adhesion force under an electric field. (e) Numerical simulation of the electric potential field lines. The voltage applied on the electrodes was 35 V. (f) Schematic of the drop impalement under an electric field.

merit could be used to manipulate a drop with fragile loading in potential applications such as in handling mammalian cells or proteins.[40]

To illustrate local wetting in response to an electric field, a drop trapping model is shown in Fig. 2f. The superhydrophobic surface can be considered as aligned pillars of silica-coated soot particles.[8,41] The nano-sized particles feature an outer radius (r) of ~60 nm and an average pore space (d_{p-p}) of ~1 μm.[41] At zero voltage, because of surface roughness and low surface energy, the drop only touched the top of the nanospheres, and a small adhesion force was observed (Fig. 2b and f). The force (F_{as}) required to pull a single nanosphere out of the air–liquid interface can be estimated from eqn (1).[41,42]

$$F_{as} = 2\pi r\gamma \cos^2 \frac{\varphi}{2} \quad (1)$$

where φ is the Young's contact angle. For a smooth fluorinated silicon wafer, φ was measured to be 115°.[8,41] Thus, F_{as} is estimated to around 8 nN for water (γ = 72 mN m^{-1}) without an applied voltage; this value is close to the value reported in the literature.[41] When voltage was applied, the L-DEP force generated from the IDA chip pulled the air-liquid interface into the porous colloidal pillars, and the contact line slid down on the nanospheres (Fig. 2f). The increase in the wetting area on the nanospheres resulted in the reduction of the contact angle (φ) and thus an increase in F_{as} (eqn 1). When the drop detached from the nanoparticle-aligned surface, F_a could be considered as the accumulation of the force from the particles along the circumference ($l = \pi D_a$) of the entire drop contact area.

$$F_a \sim F_{as} l/d_{p-p} \quad (2)$$

Herein, D_a is the drop diameter of the contact area before detachment, which can be measured by analyzing the images obtained upon the detachment of the drop. The measured diameters in response to voltage can be found in Fig. S3.† The diameter *versus* voltage curve features a relatively fast increase, followed by a plateau once the voltage exceeds 21 V. Thus, it can be predicted that the increase in the adhesion force originates from the increase of the local adhesion force and/or the detaching area. The contact angle on the nanosphere decreased as the applied voltage increased, which had the same tendency on a smooth flat surface.[36] However, rather than being confined in two dimensions in the case of a flat surface, a portion of the drop penetrated inside the

structure at elevated voltages in the case of a porous surface (Fig. 2f).

Although φ significantly reduced, the surface maintained the Cassie–Baxter state, which could be predicted from the Cassie–Baxter equation.

$$\cos\varphi_a = f_1(\cos\varphi + 1) - 1 \quad (3)$$

where f_1 is the solid fraction coefficient, which is geometric and independent of any external energy applied to the drop. For the superhydrophobic surface used herein, f_1 can be estimated from the correlation between $\cos\varphi_a$ and $\cos\varphi$ at zero voltage by eqn (3). Since φ_a = 166° and φ = 115° at zero voltage, f_1 was calculated as 0.05.

Based on the abovementioned analysis, we could establish a relation between the L-DEP force and the adhesion force. The L-DEP force results in two effects: it makes the contact line slide down along the nanospheres (reducing the contact angle) or leads to the spreading of the drop on the surface (increasing the detaching area). Both the effects increase the contact area between the liquid and the surface; this results in an increase in the adhesion force. Although there was a significant increase in the adhesion force, the surface retained its superhydrophobicity because the drop did not transition to the Wenzel state. The energy barrier required to overcome the transition was not reached since a limited voltage was applied. With the reduction of the contact angle on the nanospheres by the L-DEP force, the drop transitioned to a metastable Cassie–Baxter state. This metastable state will, however, collapse if the liquid further advances and completely covers the particles at higher voltages; this leads to a thoroughly wetted interface (the Wenzel state). For practical actuations, it is important to determine the maximum reversible adhesion force under an electric field. The breaking of the Cassie–Baxter state can be estimated from a completely immersed particle, *i.e.*, φ = 0°. From eqn (1) and (2), the theoretical maximum adhesion force on a single particle was estimated to be 27 nN, and the corresponding adhesion force was around 35 μN supposing that the contact area at detachment remained unchanged. This is the maximum adhesion force that can be reached by an electric field in the metastable Cassie–Baxter state. However, the nanospheres in reality are mostly randomly arranged with inhomogeneous heights and positions; this makes the maximum adhesion force smaller than the predicted value.

3.2. Manipulation of the dynamic interaction between the drop and the surface under an electric field

Taking advantage of the effective adhesion force modulation under an electric field, active control of the dynamic behavior, *i.e.*, the rebounding of the drop, of the drop was realized on the superhydrophobic surface. The images of the rebounding drops, as depicted in Fig. 3a, demonstrate the

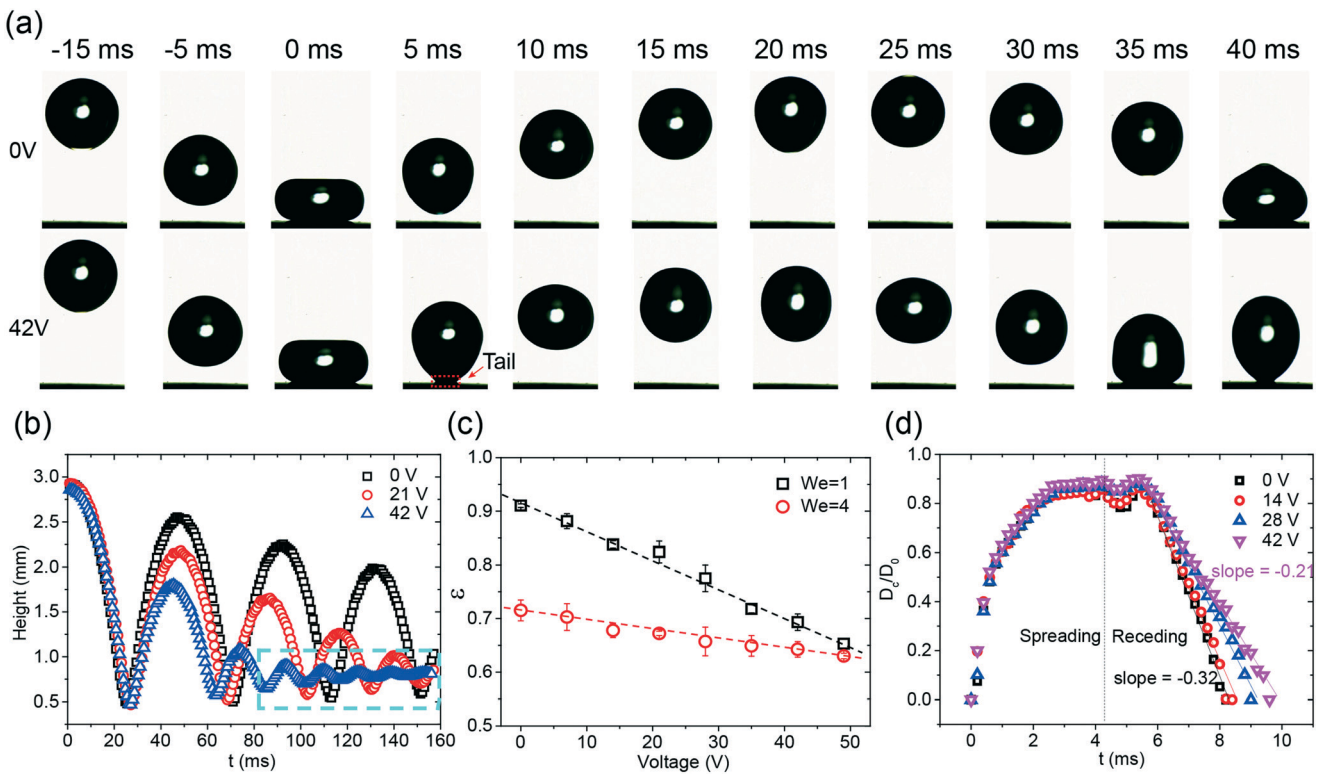

Fig. 3 Dynamic interactions between the drop and surface under an electric field. (a) The images of the rebounding drops with/without applying the voltages on the electrodes. (b) The trajectories of the drops at 0 V, 21 V, and 42 V. (c) The coefficient of restitution as a function of voltage at We = 1 and 4. (d) Diameter ratio as a function of time at various voltages ranging from 0 V to 42 V.

influence of the electric field on the drop impact. In this case, the impact velocity of the drop was 0.2 m s^{-1}, and the corresponding We was equal to unity. Without the applied voltage, after the drop released, the drop impacted the surface and smoothly rebounded (Video S2†); this was consistent with the results reported in other studies.[8] When a voltage (*i.e.* 42 V) was applied to the chip, the chip became sticky to the drop. A tail was observed during the rebounding process (Fig. 3a, Video S2†). This sticky effect indicated that an attracting force was exerted on the drop during the impact.

To quantify the effect of the electric field on drop rebounding, the time series of the rebounding drops was analyzed by the trajectories of the drop centroid (Fig. 3b). Without an external field, the drop rebounded several times, and the amplitude of rebounding slightly decreased with an increase in the number of rebounding cycles; this indicated that a small amount of energy dissipated during the impact. When the applied voltage was increased, the amplitude in each corresponding rebounding cycle as well as the period of that cycle decreased. The drop only rebounded twice in the case of 42 V. Note that the small oscillation at 42 V represents the oscillation of the drop rather than the rebounding (Fig. 3b, Video S2†). The reduction of the amplitude indicated that an increasing amount of energy was lost during rebounding at elevated voltages.

To quantify the energy loss, the coefficient of restitution ($\varepsilon = v_r/v$) in the first rebounding was measured (Fig. 3c). Herein, v_r is the velocity directly after rebounding. Because the impacting velocity would change the coefficient of restitution, two different initial heights, *i.e.* 3 mm and 9 mm, were tested in the experiments (Videos S2 and S3†). The corresponding We is equal to 1 and 4. The rebounding of a drop on a superhydrophobic coating has been previously studied.[12,13] The higher coefficient of restitution at the lower initial height agrees with the previous study.[12] For We = 1, ε significantly decreased from 0.91 at 0 V to 0.65 at 49 V. When We increased to 4, a smaller effect of the electric field on the energy dissipation was observed. ε decreased only by 0.05, namely, from 0.7 to 0.65, when a voltage of 49 V was applied. Notably, the decreasing speeds of ε in both cases are close to constants, indicated by the dashed line shown in Fig. 3c. The monotonic reduction of ε indicates that the variation of the electric field is an ideal method to tune the drop rebounding.

To verify the effect of the electric field on the rebounding, we further investigated the contact diameter ratio ($C_r = D_c/D_0$) at the first rebounding at various voltages ranging from 0 V to 42 V. Herein, D_c is the contact diameter of the drop, and D_0 is the diameter of the impacting drop. The contact diameter of the drop reflects the energy dissipation of the

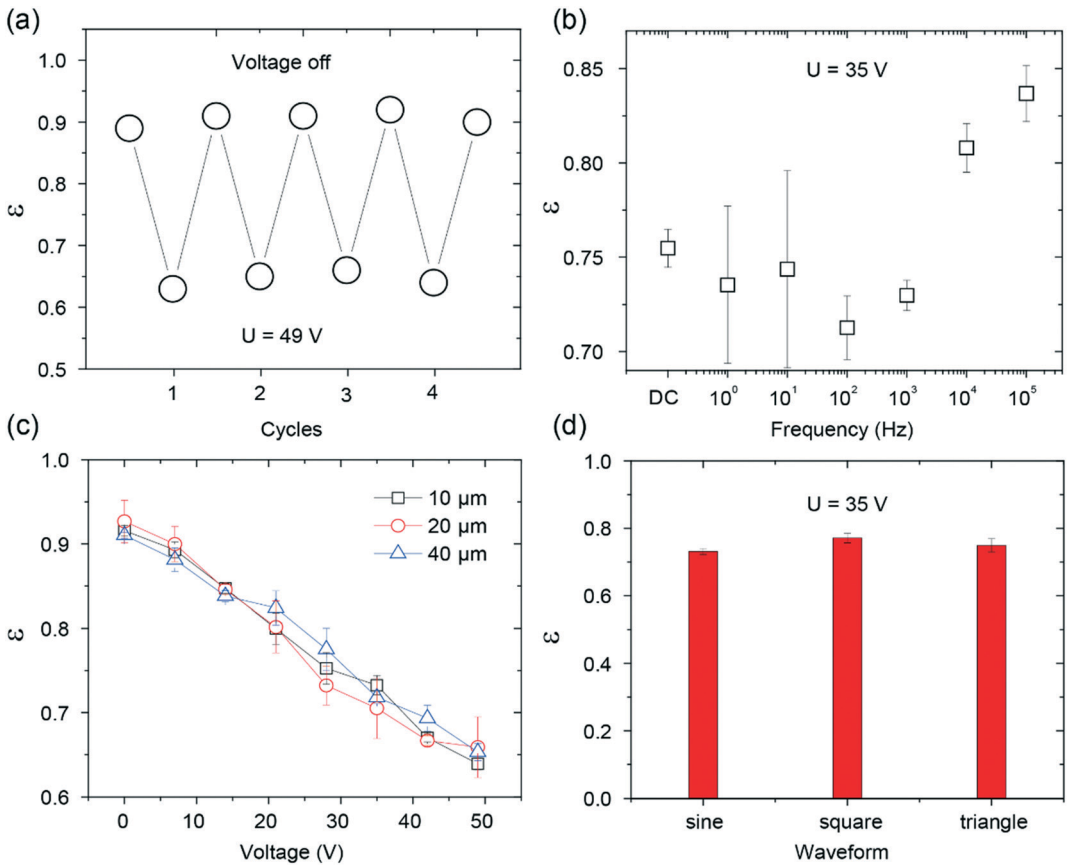

Fig. 4 Repeatability and influence of the experimental conditions on the rebounding. (a) Reversible effect of the electric field on the rebounding. (b–d) Influence of frequency, the width of electrodes, and the type of waveform on the restitution coefficient of rebounding.

impacting drop in the spreading and retraction dynamics. As shown in Fig. 3d, the electric field imposes a relatively small influence on the spreading stage. The curves obtained at different voltages are almost identical. However, the retraction dynamics show a pronounced dependence on the applied voltage; this is reflected by the change in the retraction speed. The slope increased from −0.33 to −0.21 when the voltage was increased from 0 V to 42 V. The conclusions drawn from Fig. 3d are at least threefold. First, the small influence of the electric field on the spreading phase indicates that the L-DEP force only occurs once the drop interacts with the porous-structured surface. This finding is not unexpected since the electric field highly confines itself inside the superhydrophobic coating and decays fast while penetrating above. This is in accordance with the findings obtained *via* the adhesion force analysis. Second, the growing retraction rate with the increasing voltage indicates that a higher adhesion force is imposed on the liquid surface during the receding phase. The accumulative effect of the electric field leads to an increase in the contact time and a reduction of v_r. This outcome is finally reflected by the decrease in the rebounding high; this makes the variation of the electric field an effective method for tuning the drop rebounding. Third, the imposed force is found to be uniform along the surface; this is reflected by the close to constant retraction rate. This uniform effect ensures a consistent response in the drop rebounding, making this electric-field-based tuning of the drop rebounding a reliable method.

For practical applications, it is important to consider the reversible response as well as the experimental conditions in the electric-field-dependent tuning of the drop rebounding (Fig. 4). Similar to the reversible effect of the electric field on the adhesion force, the rebounding of the drop was also found to be repeatable (Fig. 4a). The experimental conditions, such as the width of electrodes, the frequency of the applied voltages, and the type of waveforms, could have an influence on the rebounding.[28,43] To verify this, we investigated the rebounding coefficient under different conditions. The results are summarized in Fig. 4b–d. The rebounding coefficient *versus* voltage curve for different widths of the electrodes and waveforms are almost identical; this indicates that the width of the electrodes and the type of the waveforms have negligible effects on the rebounding. On the other hand, the rebounding was sensitive to the frequency of the waveform. High-energy dissipation was found when the frequency was below 1 kHz. The frequency-dependent effect is in line with the results reported in the literature.[43] However, large errors were found when the frequency was below 100 Hz. This finding is not unexpected since the contact time of the drop on the superhydrophobic surface is close to 10 ms, and a frequency below 100 Hz indicates that the rebounding finishes within a single period. The change in the voltage magnitude introduces large deviations in the measured coefficient of restitution. Thus, the results reported herein were obtained under the following conditions: the electrode width of 40 μm, sinusoidal waveform, and the frequency of 1 kHz.

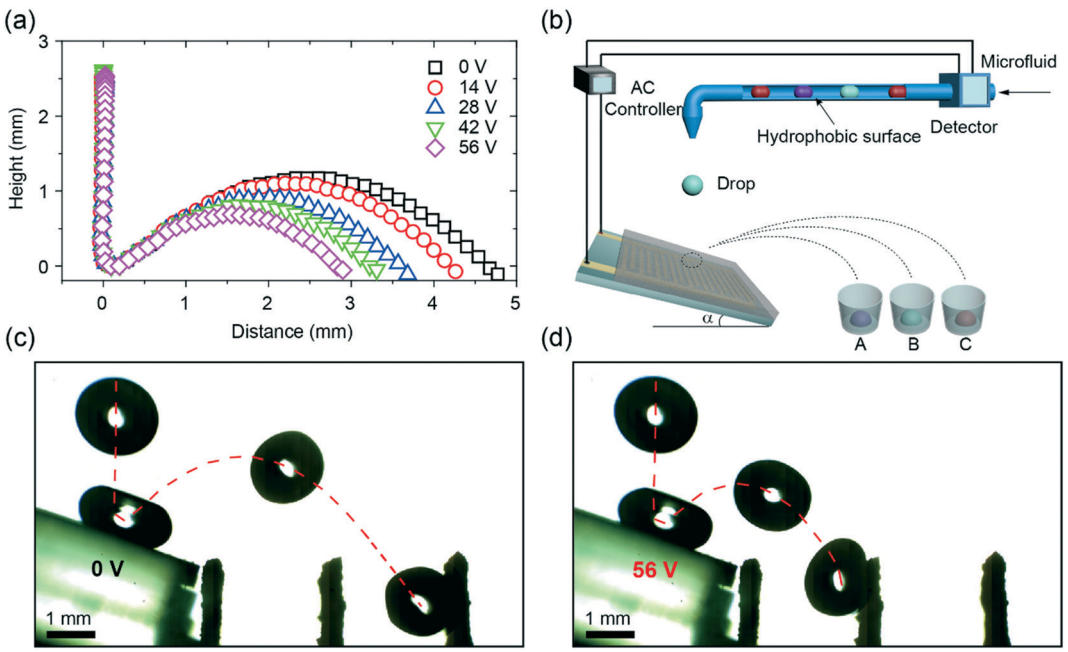

Fig. 5 Demonstration of electric-field dependent drop selector. (a) Drop bouncing distance as a function of the applied voltages. (b) Schematic of the IDA electrodes covered with the superhydrophobic coating for potential application in drop selections. (c) Time-lapsed images of the water drop bouncing on a tilted superhydrophobic coating with IDA electrodes at zero voltages. The drop jumped at a certain distance, with trajectories indicated by the red dash line, and finally fell into a channel placed in front of the chip. (d) The rebounding of the drop at the voltage of 56 V. The jumping distance decreased, and the drop fell into another channel closer to the chip.

3.3. Demonstration of the drop selector

To demonstrate the applications of dielectrowetting on the superhydrophobic surface, we performed a proof-of-concept experiment of drop sorting. A drop of water was released into a tilted superhydrophobic coating with IDA electrodes. The slope of the surface was optimized to 20° (Fig. S4†). We showed that even relatively small voltages (0–56 V) applied to the IDA could significantly change the jumping distance (Fig. 5a). Based on the monotonic relation between the jumping distance and the applied voltage, a collecting device was added to separate different drops with different jumping distances (Fig. 5b). The time-lapsed images of drop rebounding on an electric-field-controlled tilted superhydrophobic IDA chip (Fig. 5c and d) show the capacity of this device to separate the drops. Without the applied voltage, the drop jumped at a certain distance and finally fell into a channel placed in front of the chip. In contrast, the jumping distance of the drop significantly decreased at the voltage of 56 V, and the drop fell into another channel closer to the chip. A video, demonstrating the reproducibility of the separating drops, can be found in Video S4.† Due to the fast response, the small amplitude of the voltage, the non-contact of electrodes, and the superhydrophobic property of the system, the device can easily be applied to biological samples in diverse applications.

4. Conclusion

Herein, we proposed a new method to actively control the behaviors of a drop on a superhydrophobic surface by dielectrowetting at low voltages. The adhesion force and the coefficient of restitution curve were measured to elucidate the static and dynamic interactions between the drop and the surface. The adhesion force range can be reversibly tuned in the order of 15 μN at the voltage of 49 V. The modulation of the adhesion force can be easily extended to applications in digital microfluidics such as in transferring the drops, guiding the drop movement, and trapping the drops at desired places. We also demonstrated a contactless and fast response strategy to tune the drop rebounding dynamics. A monotonic relation between the coefficient of restitution and the voltage was established and used in a proof-of-concept drop selector. This low voltage response and all superhydrophobic condition by dielectrowetting may enable new applications in lab-on-drop platforms.

Conflicts of interest

There are no conflicts to declare.

Acknowledgements

We thank Prof. Limei Xu (University of Electronic Science and Technology of China) for sharing the equipment. This work was supported by the Ministry of Science and Technology, Taiwan, under Grant NSC 103-2112-M-002-008-MY3. X. D. acknowledge the funding supported provided by the National Natural Science Foundation of China (21603026) and supported by Max-Planck-Gesellschaft (Max Planck Partner Group UESTC-MPIP).

References

1 L. Mishchenko, B. Hatton, V. Bahadur, J. A. Taylor, T. Krupenkin and J. Aizenberg, *ACS Nano*, 2010, **4**, 7699–7707.
2 D. B. van Dam and C. Le Clerc, *Phys. Fluids*, 2004, **16**, 3403–3414.
3 A. L. Yarin, *Annu. Rev. Fluid Mech.*, 2006, **38**, 159–192.
4 X. Yang, J. Song, H. Zheng, X. Deng, X. Liu, X. Lu, J. Sun and D. Zhao, *Lab Chip*, 2017, **17**, 1041–1050.
5 M. Abdelgawad and A. R. Wheeler, *Adv. Mater.*, 2009, **21**, 920–925.
6 S. Ghosh, R. Lagraauw, S. Otten, A. Pit, C. Berendsen, J. Zeegers, D. Van Den Ende and F. Mugele, *Nat. Commun.*, 2014, **5**, 3559.
7 J. Seo, S.-K. Lee, J. Lee, J. S. Lee, H. Kwon, S.-W. Cho, J.-H. Ahn and T. Lee, *Sci. Rep.*, 2015, **5**, 12326.
8 X. Deng, L. Mammen, H.-J. Butt and D. Vollmer, *Science*, 2012, **335**, 67–70.
9 Z. Chu and S. Seeger, *Chem. Soc. Rev.*, 2014, **43**, 2784–2798.
10 C. Schlaich, Y. Fan, P. Dey, J. Cui, Q. Wei, R. Haag and X. Deng, *Adv. Mater. Interfaces*, 2018, **5**, 1701536.
11 J. Song, D. Zhao, Z. Han, W. Xu, Y. Lu, X. Liu, B. Liu, C. J. Carmalt, X. Deng and I. P. Parkin, *J. Mater. Chem. A*, 2017, **5**, 14542–14550.
12 X. Deng, F. Schellenberger, P. Papadopoulos, D. Vollmer and H.-J. Butt, *Langmuir*, 2013, **29**, 7847–7856.
13 B. Zhao, X. Wang, K. Zhang, L. Chen and X. Deng, *Langmuir*, 2016, **33**, 144–151.
14 S. Lin, B. Zhao, S. Zou, J. Guo, Z. Wei and L. Chen, *J. Colloid Interface Sci.*, 2018, **516**, 86–97.
15 J. Song, M. Gao, C. Zhao, Y. Lu, L. Huang, X. Liu, C. J. Carmalt, X. Deng and I. P. Parkin, *ACS Nano*, 2017, **11**, 9259–9267.
16 H. E. Jeong, M. K. Kwak and K. Y. Suh, *Langmuir*, 2010, **26**, 2223–2226.
17 Y. Lai, X. Gao, H. Zhuang, J. Huang, C. Lin and L. Jiang, *Adv. Mater.*, 2009, **21**, 3799–3803.
18 J. Li, Z. Jing, F. Zha, Y. Yang, Q. Wang and Z. Lei, *ACS Appl. Mater. Interfaces*, 2014, **6**, 8868–8877.
19 J. Li, Y. Hou, Y. Liu, C. Hao, M. Li, M. K. Chaudhury, S. Yao and Z. Wang, *Nat. Phys.*, 2016, **12**, 606.
20 S. Pan, R. Guo and W. Xu, *Soft Matter*, 2014, **10**, 9187–9192.
21 L. Heng, T. Guo, B. Wang, L.-Z. Fan and L. Jiang, *J. Mater. Chem. A*, 2015, **3**, 23699–23706.
22 J. Wang, W. Gao, H. Zhang, M. Zou, Y. Chen and Y. Zhao, *Sci. Adv.*, 2018, **4**, eaat7392.
23 X. Hong, X. Gao and L. Jiang, *J. Am. Chem. Soc.*, 2007, **129**, 1478–1479.
24 Z. Cheng, H. Lai, M. Du, S. Zhu, N. Zhang and K. Sun, *Soft Matter*, 2012, **8**, 9635–9641.

25 X. Yao, J. Ju, S. Yang, J. Wang and L. Jiang, *Adv. Mater.*, 2014, **26**, 1895–1900.
26 X. Liu, M. Cai, Y. Liang, F. Zhou and W. Liu, *Soft Matter*, 2011, **7**, 3331–3336.
27 Y. Huang, B. B. Stogin, N. Sun, J. Wang, S. Yang and T. S. Wong, *Adv. Mater.*, 2017, **29**, 1604641.
28 H. Geng, J. Feng, L. M. Stabryla and S. K. Cho, *Lab Chip*, 2017, **17**, 1060–1068.
29 M. E. Kavousanakis, N. T. Chamakos, K. Ellinas, A. Tserepi, E. Gogolides and A. G. Papathanasiou, *Langmuir*, 2018, **34**, 4173–4179.
30 L. Chen and E. Bonaccurso, *Adv. Colloid Interface Sci.*, 2014, **210**, 2–12.
31 J. Heikenfeld and M. Dhindsa, *J. Adhes. Sci. Technol.*, 2008, **22**, 319–334.
32 R. A. Hayes and B. J. Feenstra, *Nature*, 2003, **425**, 383.
33 B. Berge and J. Peseux, *Eur. Phys. J. E: Soft Matter Biol. Phys.*, 2000, **3**, 159–163.
34 A. R. Wheeler, *Science*, 2008, **322**, 539–540.
35 A. Edwards, C. Brown, M. Newton and G. McHale, *Curr. Opin. Colloid Interface Sci.*, 2017, **36**, 28–36.
36 G. McHale, C. V. Brown, M. I. Newton, G. G. Wells and N. Sampara, *Phys. Rev. Lett.*, 2011, **107**, 186101.
37 D. Baratian, R. Dey, H. Hoek, D. van den Ende and F. Mugele, *Phys. Rev. Lett.*, 2018, **120**, 214502.
38 S. Xu, H. Ren and S.-T. Wu, *J. Phys. D: Appl. Phys.*, 2013, **46**, 483001.
39 A. Russell, W. Hsieh, K. Chen and J. Heikenfeld, *Langmuir*, 2014, **31**, 637–642.
40 S. L. Freire and B. Tanner, *Langmuir*, 2013, **29**, 9024–9030.
41 M. Ye, X. Deng, J. Ally, P. Papadopoulos, F. Schellenberger, D. Vollmer, M. Kappl and H.-J. Butt, *Phys. Rev. Lett.*, 2014, **112**, 016101.
42 A. Scheludko, B. Toshev and D. Bojadjiev, *J. Chem. Soc., Faraday Trans. 1*, 1976, **72**, 2815–2828.
43 T. B. Jones, J. D. Fowler, Y. S. Chang and C.-J. Kim, *Langmuir*, 2003, **19**, 7646–7651.

